Report on tests @ NCD-SWEET of Oct. 15-16, 2018

M. Siano,* B. Paroli, and M. A. C. Potenza

Dipartimento di Fisica, Università degli Studi di Milano and INFN Sezione di Milano, via G. Celoria, 16, 20133 Milano, Italy

(Dated: November 8, 2018)

* mirko.siano@unimi.it

I. INTRODUCTORY REMARKS

In this document, we will show the results for the speckle tests performed at ALBA NCD-SWEET beamline on Oct. 16$^{\text{th}}$ 2018.

A. Data sets

- CCD camera gain set to 99. Probed sample-detector distances: 57 mm, 67 mm, 77 mm, 87 mm, 97 mm, 127 mm, 157 mm, 180 mm, 200 mm, 250 mm, 300 mm, 350 mm, 400 mm, 450 mm. Graphs shown in this report refer to these data;

- CCD camera gain set to 9. Probed sample-detector distances: 180 mm, 200 mm, 250 mm, 300 mm, 350 mm, 400 mm, 450 mm. Analysis to be completed.

For each distance, two sets of data were acquired: one with a capillary filled with the colloidal suspension (silica nanoparticles, 500 nm diameter, nominal volume fraction 10 %), the other with a capillary filled with only water. Each acquisition consists of a stack of 100 images acquired with an exposure time of 50 ms. For each acquisition, we performed DFA with Local Oscillator compensation (namely, we divide the difference between two different images I_1 and I_2 by their sum) to retrieve the pure speckle signal i_s from images

$$i_s = \frac{I_1 - I_2}{I_1 + I_2} \tag{1}$$

and we extracted horizontal and vertical profiles from the corresponding 2D power spectra.

B. Details of optics

- YAG:Ce thickness: 100 μm;

- microscope objective magnification: 23X;

- microscope objective Numerical Aperture: 0.4;

- CCD pixel size: 3.75 μm.

C. Details of data analysis

- R.O.I.: [10:910,10:910];
- image lag for DFA: 50;
- angular sector for horizontal direction: [-10:10];
- angular sector for vertical direction: [80:100].

II. MICROSCOPE OBJECTIVE MAGNIFICATION CHECK

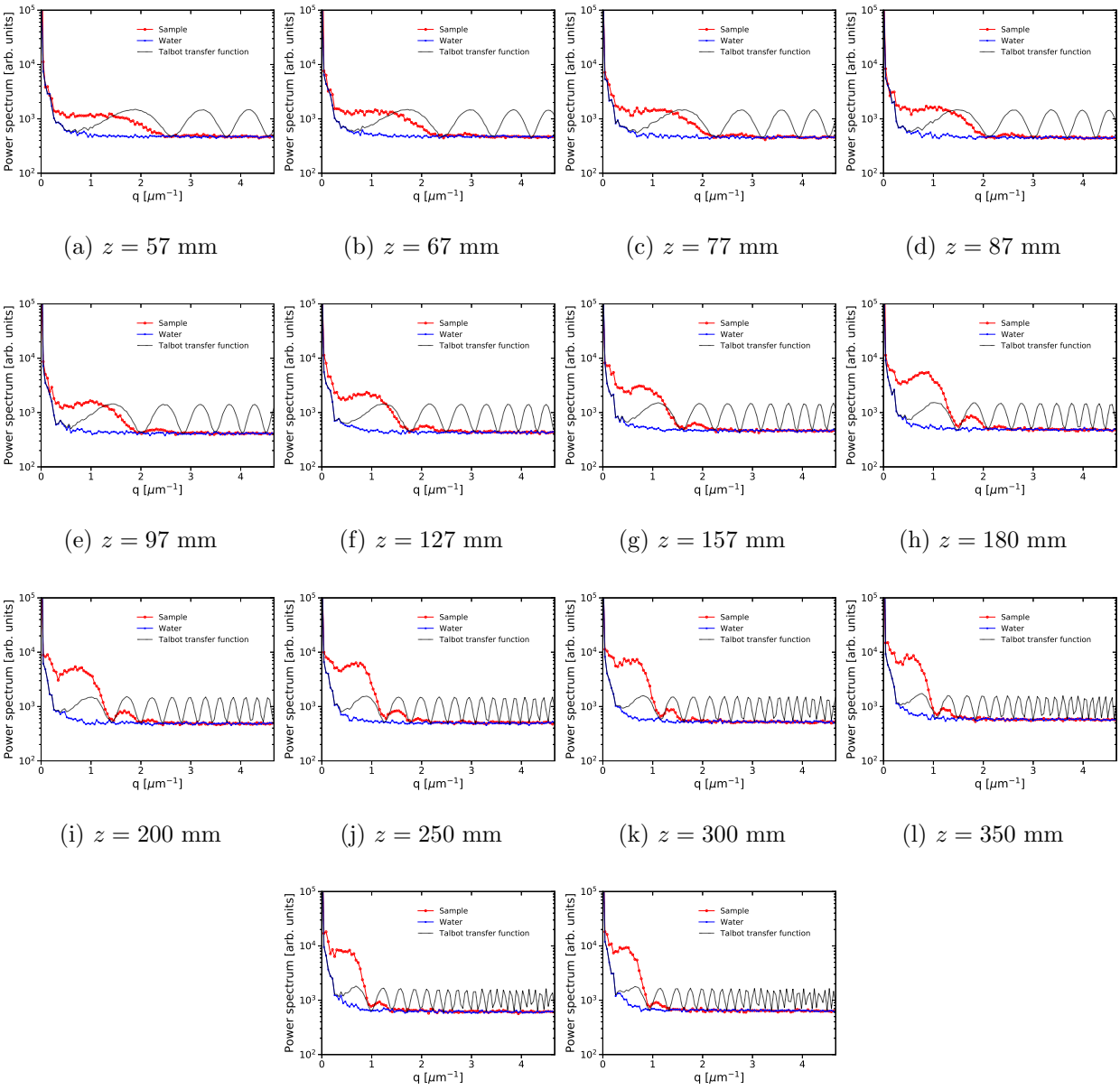

(a) $z = 57$ mm (b) $z = 67$ mm (c) $z = 77$ mm (d) $z = 87$ mm

(e) $z = 97$ mm (f) $z = 127$ mm (g) $z = 157$ mm (h) $z = 180$ mm

(i) $z = 200$ mm (j) $z = 250$ mm (k) $z = 300$ mm (l) $z = 350$ mm

(m) $z = 400$ mm (n) $z = 450$ mm

FIG. 1: Horizontal profiles of heterodyne speckle power spectra (solid red line with open red circles) and corresponding shotnoise data (solid blue line with blue square dots). The theoretical Talbot transfer function at the nominal distance z (dotted black line) is also reported for comparison.

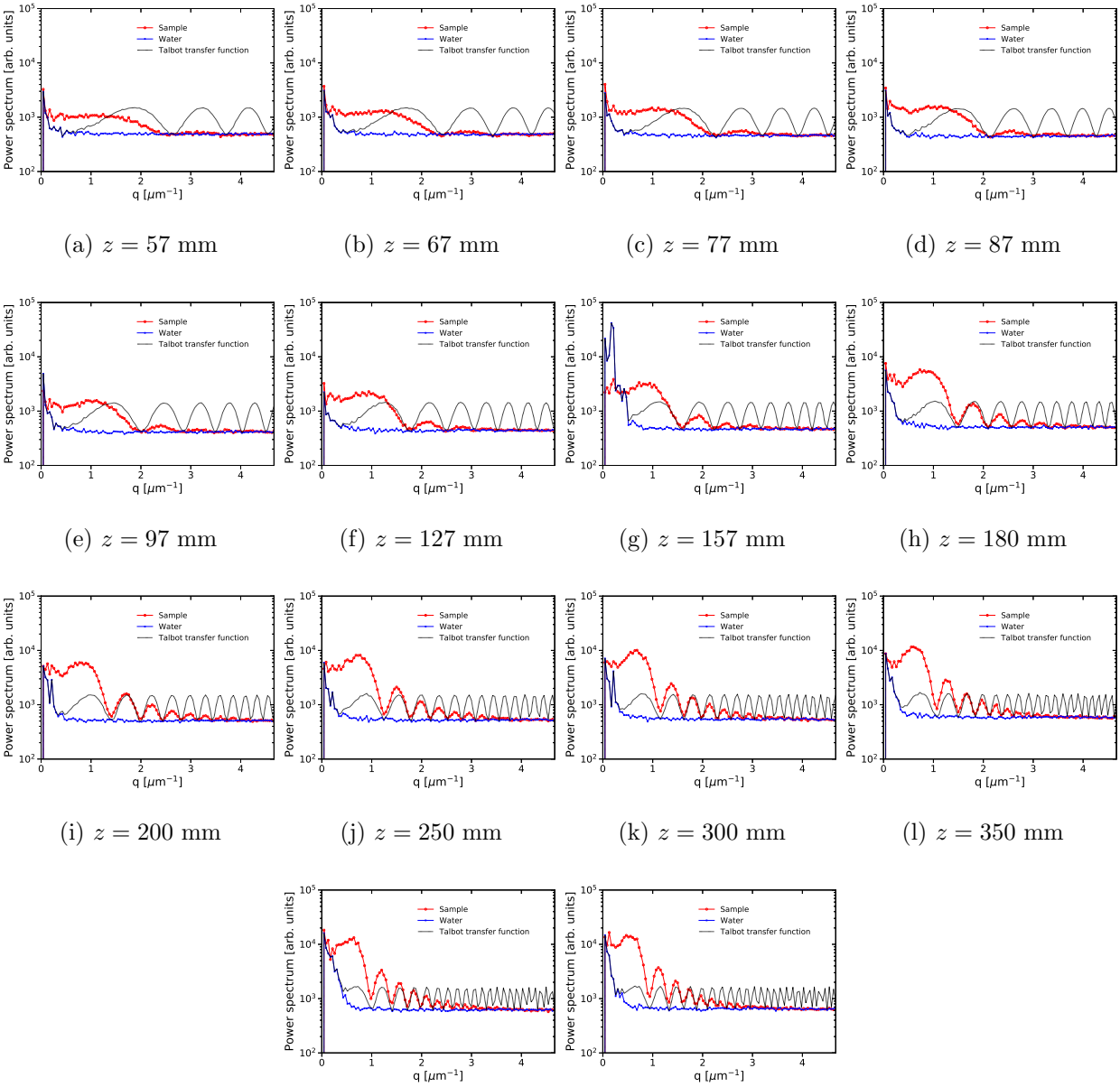

(a) $z = 57$ mm (b) $z = 67$ mm (c) $z = 77$ mm (d) $z = 87$ mm

(e) $z = 97$ mm (f) $z = 127$ mm (g) $z = 157$ mm (h) $z = 180$ mm

(i) $z = 200$ mm (j) $z = 250$ mm (k) $z = 300$ mm (l) $z = 350$ mm

(m) $z = 400$ mm (n) $z = 450$ mm

FIG. 2: Vertical profiles of heterodyne speckle power spectra (solid red line with open red circles) and corresponding shotnoise data (solid blue line with blue square dots). The theoretical Talbot transfer function at the nominal distance z (dotted black line) is also reported for comparison.

As it can be noticed from Fig. 1 and from Fig. 2 in particular, the positions of Talbot maxima and minima perfectly match the theoretical ones. This provides a robust cross-check for the microscope objective magnification ($M \sim 23$) which is in good agreement

with the value obtained from the measured Field Of View $FOV = [212\ \mu\text{m}, 160\ \mu\text{m}]$ (total image size = 1296x966 pixels, pixel size = 3.75 μm). For these numbers, refer to the email communication by Andriy on Oct. 18^{th}, 2018.

We also notice that the number of Talbot oscillations along the horizontal direction is smaller than in the vertical one. This reflects the asymmetry in 2D power spectra and it implies that coherence effects are present, at least in the horizontal direction. Here the value of the Fourier wavevector q at which power spectra reach the shotnoise level gets smaller as the sample-detector distance is increased: this is indicative of a decay of Talbot oscillations dictated by coherence.

III. CALIBRATION FUNCTION

The power spectrum $I(q)$ of heterodyne speckle field is given by:

$$I(q,z) = C(q,z)T(q,z)S(q)H(q) + P(q), \tag{2}$$

where

- $C(q,z)$ represents the squared modulus of the radiazion CCF;
- $T(q,z) = 2\sin^2[zq^2/(2k)]$ represents the Talbot transfer function;
- $S(q)$ represents the particle form factor. For small particles, it is almost constant and henceforth it can be neglected;
- $H(q)$ represents the calibration function. It is mainly given by the response function (in the reciprocal space) of the YAG screen and detection optics;
- $P(q)$ represents the shotnoise contribution.

The calibration function is obtained from the shortest sample-detector distances by dividing the acquired power spectra (upon shotnoise reduction) by the theoretical Talbot transfer function:

$$\frac{I(q,z) - P(q)}{T(q,z)} = C(q,z)H(q). \tag{3}$$

By exploiting the (possibly very) short sample-detector distances z, in the righthand side of Eq. 3 we can approximate $C(q,z) \sim 1$ due to the spatial scaling $\Delta r = zq/k$, where Δr is the argument appearing in the expression of the radiation CCF. Hence the aformentioned reduction provides a direct measurement of the spatial frequency calibration function $H(q)$. In these conditions, data from different sample-detector distances must superimpose to build the single master curve $H(q)$. If they do not, one can conclude that the radiation CCF is affecting power spectra. This is likely the case in the horizontal direction, since the vertical transverse coherence length of undulator radiation is (much) larger than the horizontal one. Data shown in Fig. 3 confirm our guess. We will then associate only vertical profiles to the calibration function $H(q)$.

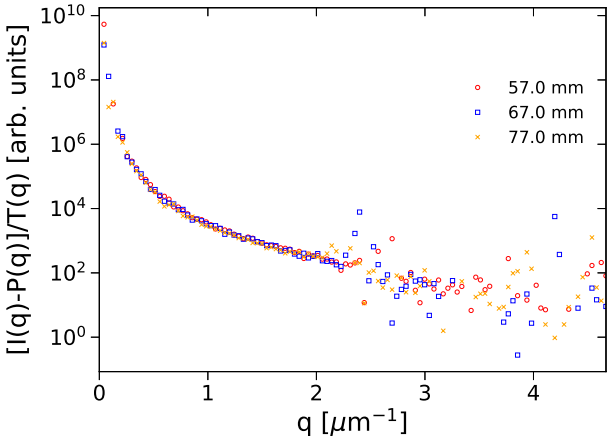

(a) Horizontal direction, $z_{\max} = 80$ mm

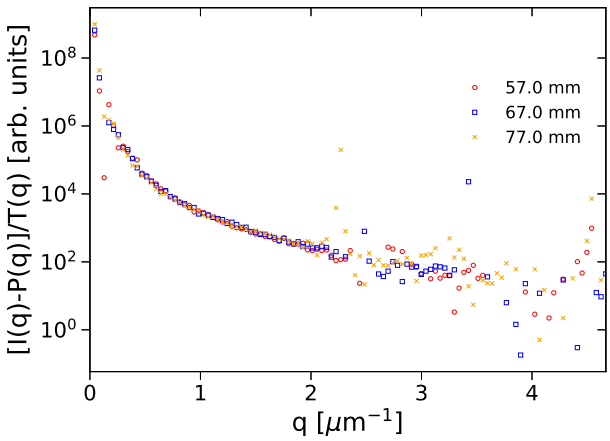

(b) Vertical direction, $z_{\max} = 80$ mm

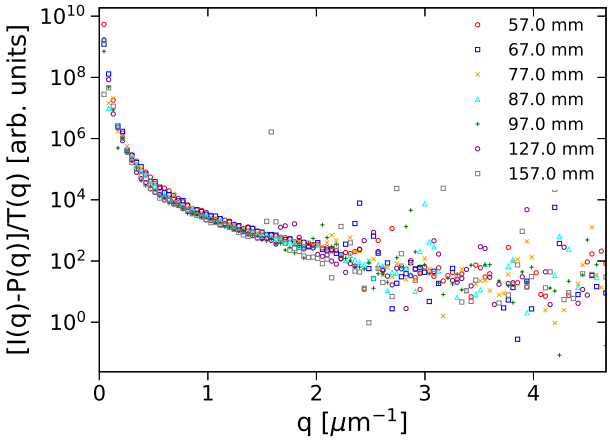

(c) Horizontal direction, $z_{\max} = 160$ mm

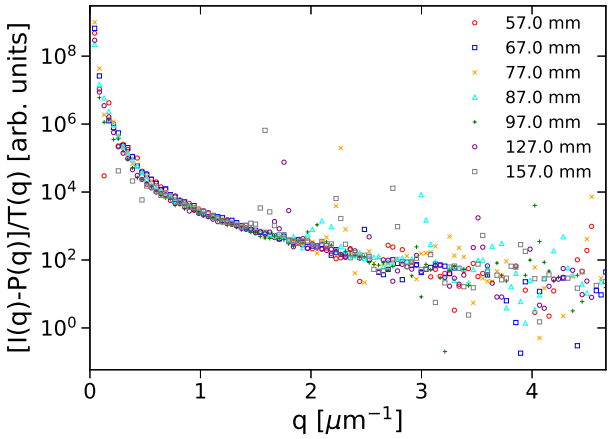

(d) Vertical direction, $z_{\max} = 80$ mm

FIG. 3: Calibration functions obtained as in Eq. 3 from (a,c) horizontal and (b,d) vertical profiles. (a,b) Only the shortest sample-detector distances 57 mm, 67 mm and 77 mm are reported. (c,d) By including also 87 mm, 97 mm and 127 mm, horizontal profiles fail to build a single master curve due to the limited spatial coherence, opposite to the case of vertical profiles.

IV. CALIBRATION ISSUES

Using the calibration function from vertical profiles as in Fig. 3(b,d) caused problems in data reduction. First of all, compensation of the Talbot transfer function $T(q, z)$ as in Eq. 3 is not optimal (even at the shortest sample-detector distance $z = 57$ mm) due to the presence of Talbot zeros within the probed wavevectors. Then, more significantly, reduced data failed to build the master curve of the radiation CCF upon the spatial scaling and they were also not properly normalized (upon calibration, data cannot exceed value 1, while reduced curves were even higher than 2).

We then adopted the following workaround for these issues: we performed a piecewise reduction of the Talbot transfer function by selecting only those wavevectors where $T(q)$ is larger than a certain threshold (hence sensibly different from zero) and we plot the results for each sample-detector distance. We then varied the value of the threshold (given in percentage of the maximum value of the Talbot transfer function $T(q, z)$) to compare the outcomes of this procedure. Results are shown in Fig. 4 and in Fig. 5 for horizontal and vertical profiles, respectively.

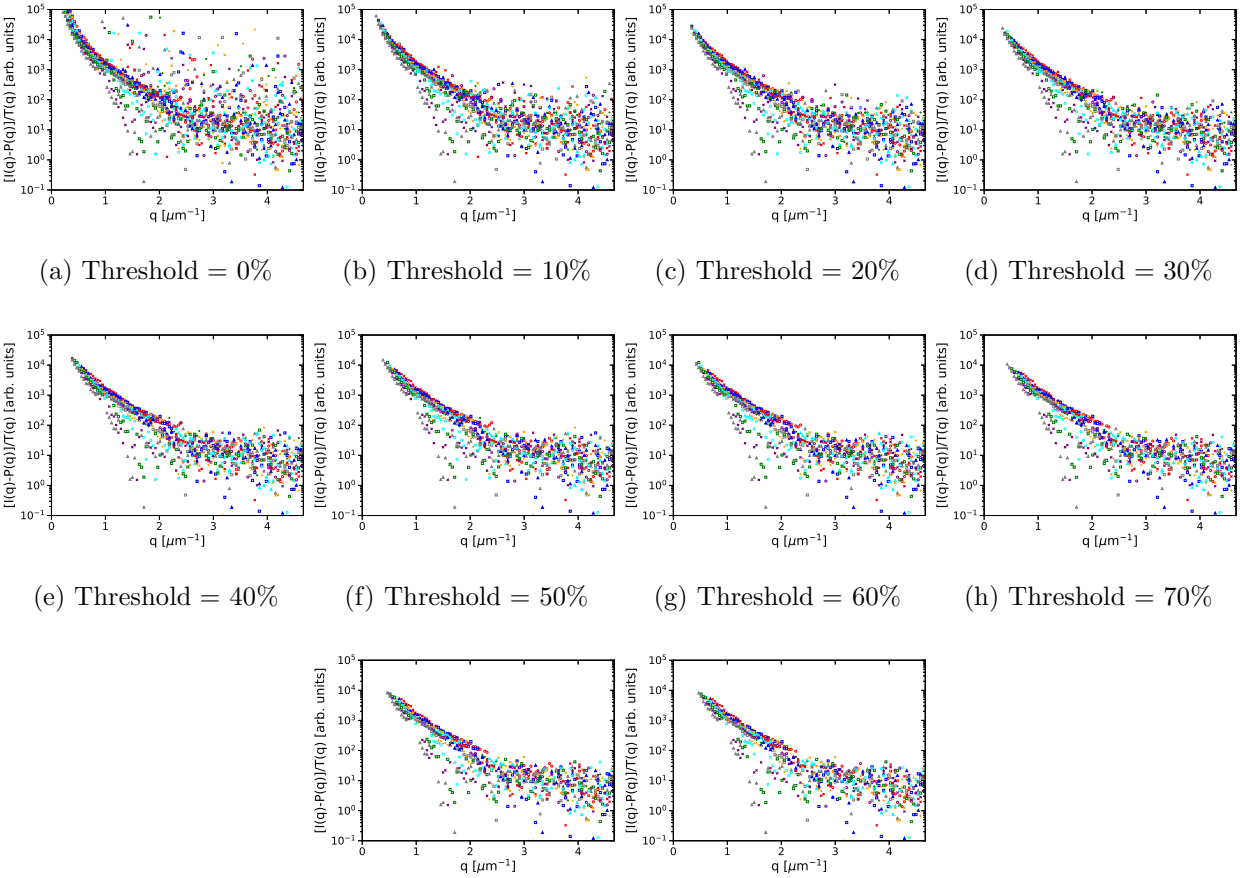

(a) Threshold = 0% (b) Threshold = 10% (c) Threshold = 20% (d) Threshold = 30%

(e) Threshold = 40% (f) Threshold = 50% (g) Threshold = 60% (h) Threshold = 70%

(i) Threshold = 80% (j) Threshold = 90%

FIG. 4: Horizontal calibration functions from a piecewise reduction of the Talbot transfer function. Threshold values are indicated as percentage of the maximum value of $T(q)$.

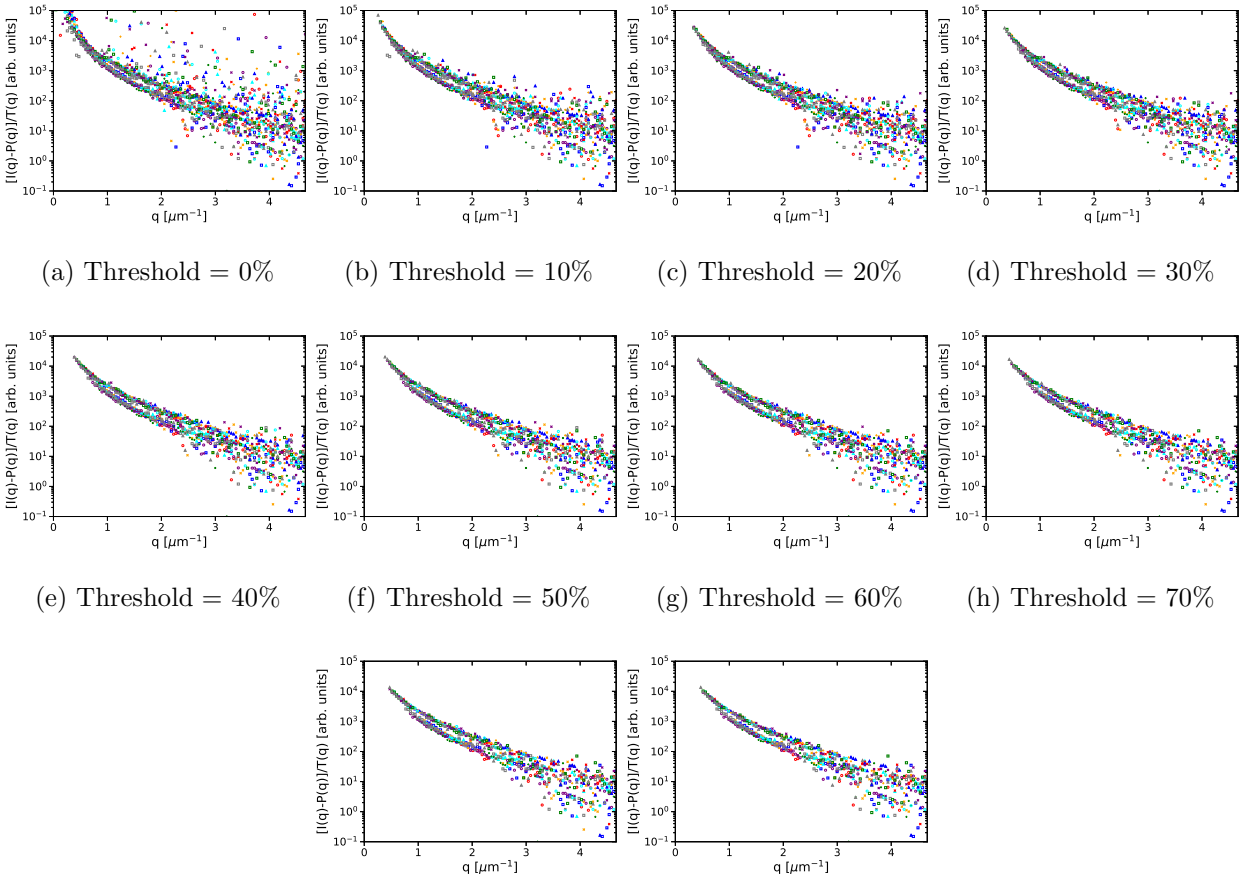

(a) Threshold = 0% (b) Threshold = 10% (c) Threshold = 20% (d) Threshold = 30%

(e) Threshold = 40% (f) Threshold = 50% (g) Threshold = 60% (h) Threshold = 70%

(i) Threshold = 80% (j) Threshold = 90%

FIG. 5: Vertical calibration functions from a piecewise reduction of the Talbot transfer function. Threshold values are indicated as percentage of the maximum value of $T(q)$.

It is evident from Fig. 4 and Fig. 5 that the piecewise reduction of the Talbot transfer function by means of threshold values is effective in avoiding division by zero. Furthermore, increasing the threshold level compensates for the spurious contributions arising near Talbot minima and leads to high-quality curves.

With reference to Fig. 4, it can be noticed how horizontal profiles at larger z fail to superimpose. As the detection plane is moved away from the sample, they become increasingly narrower due to the limited spatial coherence.

Vertical profiles from Fig. 5 unexpectedly exhibit two different master curves. The one standing higher corresponds to sample-detector distances within 180 mm and 450 mm, while the one standing lower corresponds to z ranging between 57 mm and 157 mm. This is exactly what caused the subsequent data reduction to fail: opposite to what is usually done, in this case we cannot use the calibration function obtained from the shortest distances to reduce data at larger distances.

Why do data from different data sets build two different calibration curves? To answer this question, we performed a quantitative characterization of the two calibration functions. Restricting ourselves to $q > 1$ μm^{-1}, and considering only z=57 mm, 67 mm, 77 mm, 87 mm, 97 mm for one curve (labeled as 1) and z=180 mm, 200 mm for the other one (labeled as 2), data resemble a negative exponential of the form

$$H(q) \propto \exp\left(-\frac{q}{q_{\text{scint}}}\right), \tag{4}$$

as shown in Fig. 6

The characteristic wavevectors q_{scint} are different for the two data sets (0.61 μm^{-1} for the first curve, 0.49 μm^{-1} for the second one), and they are associated to characteristic length scales $L_1 = 2\pi/q_{\text{scint},1} = 10$ μm and $L_2 = 2\pi/q_{\text{scint},2} = 13$ μm, respectively. This observation, together with the results from Oct. 15^{th} regarding speckle contrast vs defocusing, points toward a reduced spatial resolution due to small changes in the position of the focal plane with respect to the YAG front face location. Indeed, it is worth noticing that data corresponding to larger distances were acquired before 14h25m, roughly the time when we had a skype call to discuss about the ongoing experiments. We then agreed to move closer to the sample (data at shorter distances were acquired after 15h18m) and this change in the setup might have altered the focusing conditions with respect to earlier measurements.

However, thanks to the large coherence in the vertical direction, we are able to retrieve

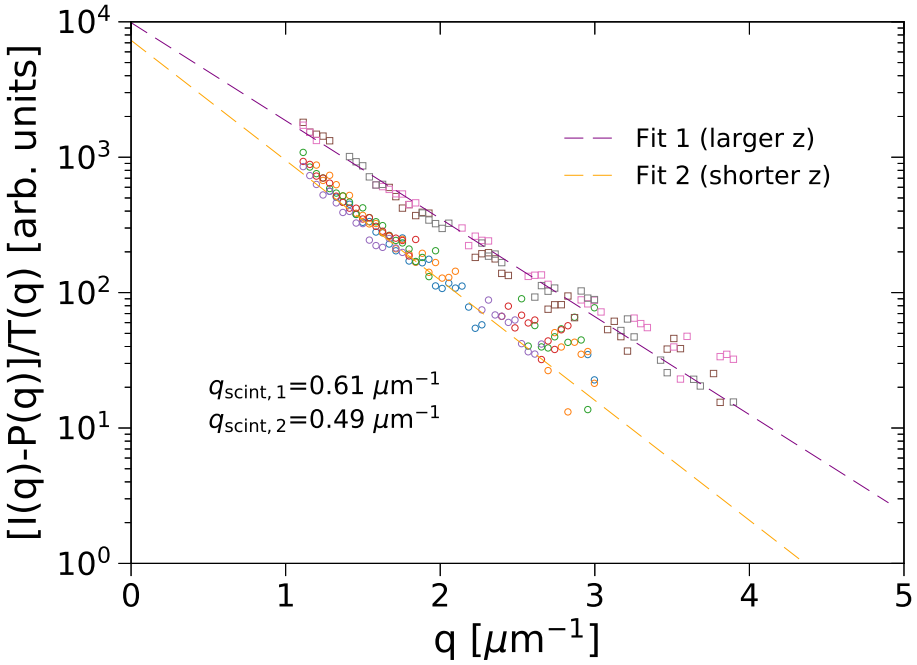

FIG. 6: Calibration curves for larger (open squares) and shorter (open circles) distances and corresponding negative exponential fit according to Eq. 4 (dashed purple line and dashed orange line, respectively). Larger distances are labeled with 1, while shorter distances are labeled with 2. The fitted values of q_{scint} are reported for completeness.

the correct calibration function for both data sets, and we can use one curve to process distances shorter than 180 mm and the other one to process larger distances. In this way normalization of power spectra and Talbot oscillations is restored, as it is shown in Fig. 7 and Fig. 8. It proves that, as long as speckles are present, coherence information can be consistently retrieved regardless of (limited) defocus aberration, provided that the corresponding calibration function is determined. Also, by comparing data at different sample-detector distances and by exploting the master curve criterion for $H(q)$, we are able to retrieve the calibration function even when we cannot move closer to the sample due to mechanical limitations (for ESRF data, calibration was performed by moving a few millimeters downstream the scattering sample). This two observations prove the robustness and self-consistency of the technique.

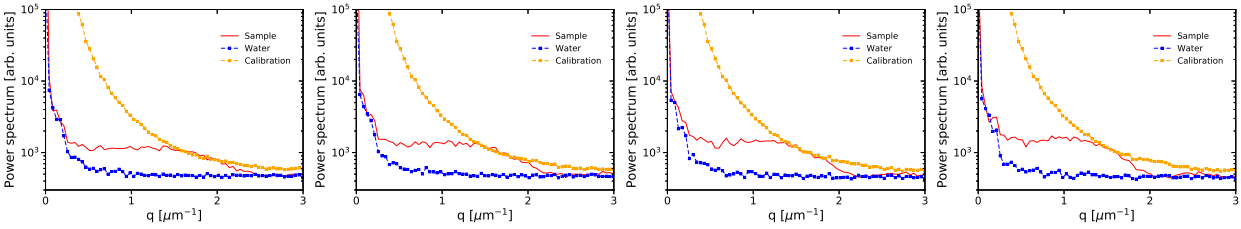

(a) $z = 57$ mm (b) $z = 67$ mm (c) $z = 77$ mm (d) $z = 87$ mm

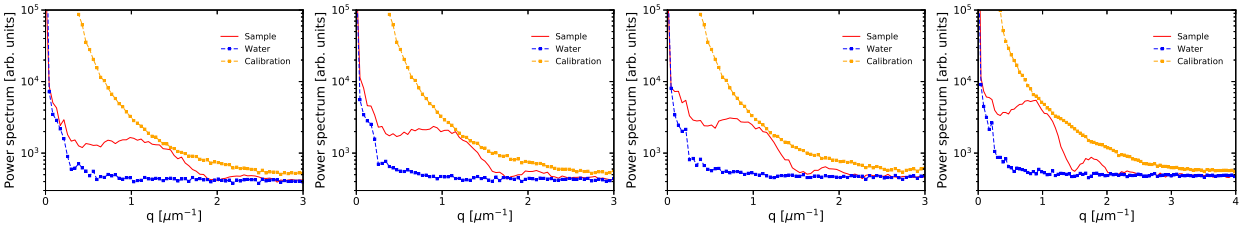

(e) $z = 97$ mm (f) $z = 127$ mm (g) $z = 157$ mm (h) $z = 180$ mm

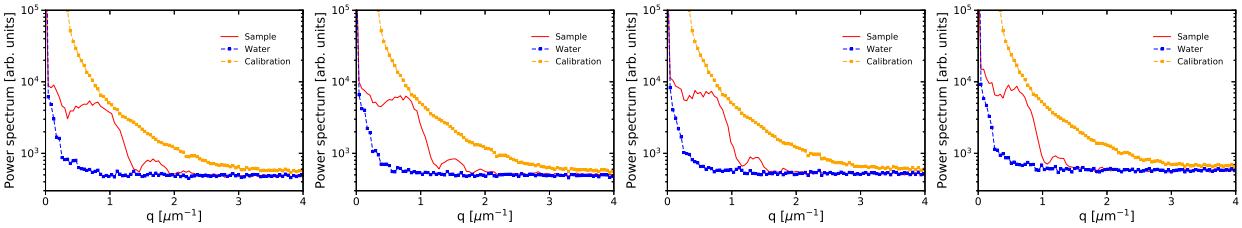

(i) $z = 200$ mm (j) $z = 250$ mm (k) $z = 300$ mm (l) $z = 350$ mm

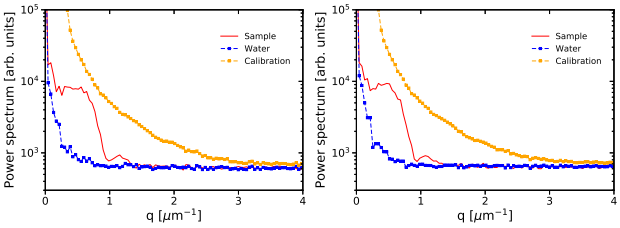

(m) $z = 400$ mm (n) $z = 450$ mm

FIG. 7: Horizontal profiles of acquired power spectra (solid red line with open red circles). We also report the results for data from a capillary filled with only water (dashed blue line with blue square dots), as well as the spatial frequency calibration function of the YAG screen and detection optics (dashed orange line with orange square dots).

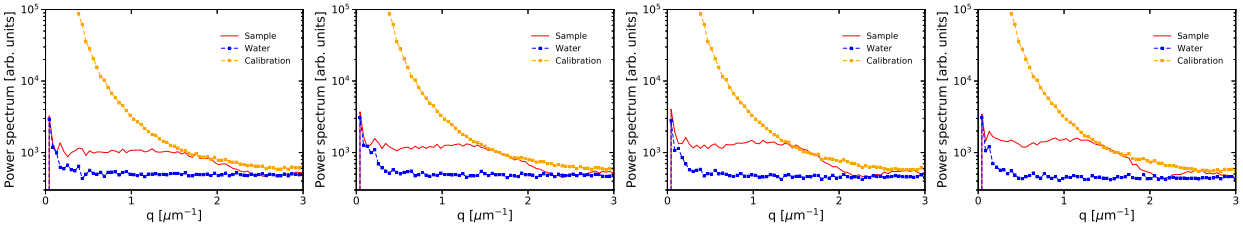

(a) $z = 57$ mm (b) $z = 67$ mm (c) $z = 77$ mm (d) $z = 87$ mm

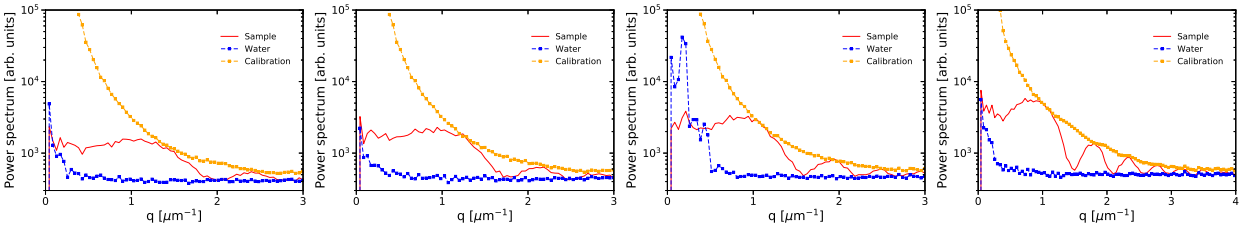

(e) $z = 97$ mm (f) $z = 127$ mm (g) $z = 157$ mm (h) $z = 180$ mm

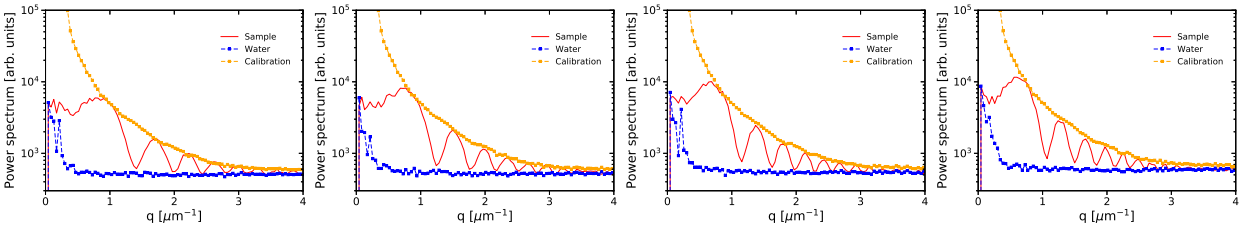

(i) $z = 200$ mm (j) $z = 250$ mm (k) $z = 300$ mm (l) $z = 350$ mm

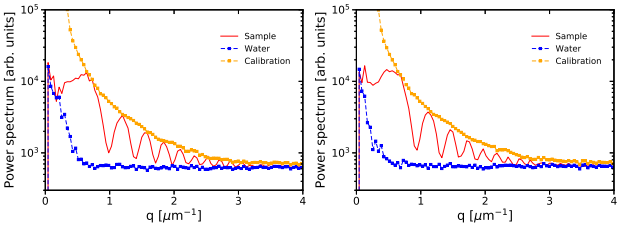

(m) $z = 400$ mm (n) $z = 450$ mm

FIG. 8: Vertical profiles of acquired power spectra (solid red line with open red circles). We also report the results for data from a capillary filled with only water (dashed blue line with blue square dots), as well as the spatial frequency calibration function of the YAG screen and detection optics (dashed orange line with orange square dots).

V. FROM TALBOT OSCILLATIONS TO THE RADIATION CCF

After shotnoise subtraction, calibration reduction and spatial scaling, power spectra at different sample-detector distances superimpose on a spatial master curve in the horizontal direction. In fact, Talbot maxima lie on (and thus identify) a single curve. The spatial master curve is not easily recognizable along the vertical direction since the envelopes of Talbot oscillations start to be influenced by the walkoff effect related to the finite sensor size. Results are shown in Fig. 9.

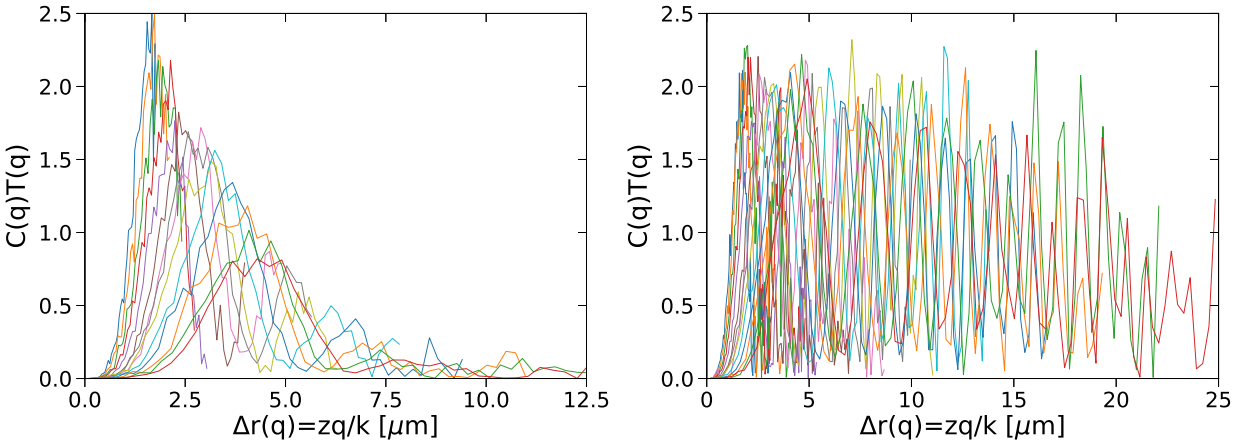

(a) Horizontal direction

(b) Vertical direction

FIG. 9: (a) Horizontal and (b) vertical profiles of acquired power spectra after shotnoise and calibration reduction. Notice the spatial scale on the x-axis, implying that the master curve in the horizontal direction is representative of the radiation CCF. Along the vertical direction the spatial master curve is not as clearly visible due to the walkoff effect.

One can compensate for the walkoff effect (and in general extract the radiation CCF from the curves $C(\Delta r)T(\Delta r)$) through the following steps:

- extract Talbot maxima and minima from the measured curves $C(\Delta r)T(\Delta r)$;
- compute the radiation CCF as the average between binned maxima and minima (labeled as 1 in the following);
- compute the radiation CCF as by reducing binned maxima for the walkoff effect (labeled as 2 in the following). If no other phenomenon other than the walkoff induced

by the finite sensor is affecting Talbot oscillations, this reduction should give the same result as the previous point.

The results of these last steps are reported in Fig. 10 and Fig. 11, where in the latter we also fitted data with a Gaussian function of the form

$$|\mu(\Delta r)| = e^{-\frac{\Delta r^2}{\sigma^2}}. \tag{5}$$

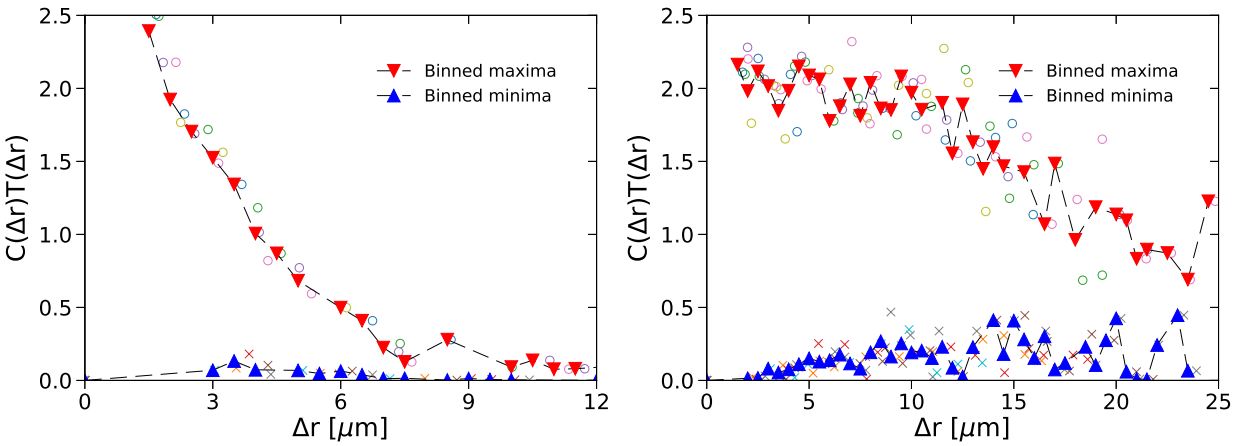

(a) Horizontal direction

(b) Vertical direction

FIG. 10: (a) Horizontal and (b) vertical Talbot maxima and minima. Spatial master curve of the radiation CCF can be recognized in both cases.

Fitted values for σ are

- $\sigma_{\text{hor},1} = (4.7 \pm 0.1)\ \mu\text{m}$
- $\sigma_{\text{hor},2} = (4.6 \pm 0.2)\ \mu\text{m}$
- $\sigma_{\text{ver},1} = (32.2 \pm 2.6)\ \mu\text{m}$
- $\sigma_{\text{ver},2} = (35.8 \pm 4.3)\ \mu\text{m}$

The transverse coherence length (as defined by Mandel) is given by $\sigma_{\text{coh}} = \sigma\sqrt{\pi}$:

- $\sigma_{\text{coh,hor},1} = (8.3 \pm 0.2)\ \mu\text{m}$
- $\sigma_{\text{coh,hor},2} = (8.1 \pm 0.4)\ \mu\text{m}$

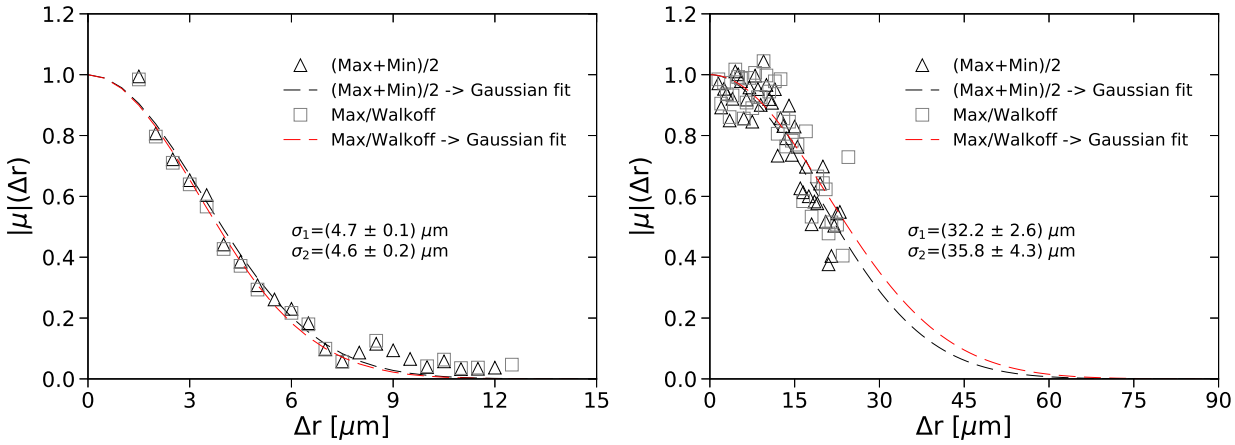

(a) Horizontal direction

(b) Vertical direction

FIG. 11: (a) Horizontal and (b) vertical radiation CCF, obtained as the average between binned maxima and minima (open black triangles, labeled as 1) and as the ratio between binned maxima and the walkoff term (open gray squares, labeled as 2). We also report a Gaussian fit according to Eq. 5 . The fitted values of σ for both cases are indicated.

- $\sigma_{\mathrm{coh,ver,1}} = (57.1 \pm 4.6)\ \mu$m
- $\sigma_{\mathrm{coh,ver,2}} = (63.5 \pm 7.6)\ \mu$m

Assuming the VCZ theorem holds, the beam size is related to the transverse coherence length previously defined by the following relation:

$$\sigma_{\mathrm{BEAM}} = \lambda z/(2\sqrt{\pi}\sigma_{\mathrm{coh}}), \tag{6}$$

where this time z is the distance of the scattering sample from the undulator center (33 m for our experiment):

- $\sigma_{\mathrm{BEAM,hor,1}} = (112 \pm 3)\ \mu$m
- $\sigma_{\mathrm{BEAM,hor,2}} = (115 \pm 6)\ \mu$m
- $\sigma_{\mathrm{BEAM,ver,1}} = (16.3 \pm 1.3)\ \mu$m
- $\sigma_{\mathrm{BEAM,ver,2}} = (14.7 \pm 1.8)\ \mu$m